PHYSICAL REVIEW B VOLUME 52, NUMBER 8 15 AUGUST 1995-II

Monte Carlo simulation of electron drift velocity in low-temperature-grown gallium arsenide in a Schottky-barrier model

P. Arifin, E. Goldys, and T. L. Tansley

Semiconductor Science and Technology Laboratories, Physics Department, Macquarie University, New South Wales 2109, Australia

(Received 16 November 1994; revised manuscript received 7 April 1995)

We present a method of simulating the electron transport in low-temperature-grown GaAs by the Monte Carlo method. Low-temperature-grown GaAs contains microscopic inclusions of As and these inhomogeneities render impossible the standard Monte Carlo mobility simulations. Our method overcomes this difficulty and allows the quantitative prediction of electron transport on the basis of principal microscopic material parameters, including the impurity and the precipitate concentrations and the precipitate size. The adopted approach involves simulations of a single electron trajectory in real space, while the influence of As precipitates on the GaAs matrix is treated in the framework of a Schottky-barrier model. The validity of this approach is verified by evaluation of the drift velocity in homogeneous GaAs where excellent agreement with other workers' results is reached. The drift velocity as a function of electric field in low-temperature-grown GaAs is calculated for a range of As precipitate concentrations. Effect of compensation ratio on drift velocity characteristics is also investigated. It is found that the drift velocity is reduced and the electric field at which the onset of the negative differential mobility occurs increases as the precipitate concentration increases. Both these effects are related to the reduced electron mean free path in the presence of precipitates. Additionally, comparatively high low-field electron mobilities in this material are theoretically explained.

I. INTRODUCTION

Recently there has been an increased interest in transport properties of thin epitaxial layers of GaAs grown by molecular-beam epitaxy at low (bout 200 °C) substrate temperatures.[1] Low-temperature-grown GaAs (LT GaAs) undergoes substantial morphological changes during thermal annealing, becoming highly resistive, 10^7 Ω cm having been reported.[2] This property has suggested applications as a buffer layer in various GaAs-based devices, including metal-semiconductor field-effect transistors (MESFET's) and high-electron-mobility transistors (HEMT's). The use of a LT GaAs buffer layer allows a virtual elimination of sidegating and backgating of individual devices on a chip while maintaining integration density, and this discovery has triggered wide-ranging studies of LT GaAs.[3] The defect structure of the as-grown and the annealed material has been examined.[4,5] Growth conditions are very far from those required for high-quality material and numerous defect levels ensue. In LT GaAs annealed under appropriate conditions, however, a significant fraction of such defects seem to disappear and x-ray studies show very high crystalline quality. Structural studies by transmission electron microscopy (TEM) reveal the presence of precipitates,[6] believed to be composed of metallic arsenic, since LT GaAs is nonstoichiometric with approximately 1% of excess arsenic. It has been proposed that the presence of these As precipitates dominates the electronic properties of the annealed material, although controversy remains as to the nature of electronic transport.[6-8]

Studies of fundamental properties of LT GaAs have been conducted in parallel with applications in various areas of solid-state optoelectronics. Several interesting devices based on LT GaAs have been proposed that exploit the unique characteristics of this composite material.[9] In particular, the less than 1 ps carrier lifetime in LT GaAs has generated interest in very fast metal-semiconductor-metal (MSM) LT GaAs detectors.[10] This short lifetime, combined with high resistivities, has motivated the construction of fast photoconductive switches capable of picosecond switching of voltages up to 1000 V that had not previously been possible.[11] LT GaAs may then become a key element of several devices in important and expanding areas of optoelectronics technology, principally in fast signal generation and detection.

The operation of such classes of devices often subjects LT GaAs to electric fields greater than 10^4 V cm^{-1},[11] and an understanding of high-field transport characteristics is therefore needed. In this paper we offer such a microscopic description on the basis of the Monte Carlo (MC) simulation. The principal microscopic parameters in this calculation are the concentration and the size distribution of As precipitates, as determined experimentally by TEM measurements, and the concentration of shallow impurities. The key advantage of a MC simulation approach over the evaluation of mobility on the basis of the transport scattering cross section of a single precipitate is the possibility of including correlations between individual scattering events, important when the concentration of the precipitates is large, the most interesting regime from the experimental point of view. Other experimental problems addressed in our calculations are also relevant from the point of view of applications. We explore the high-electric-field region where negative differential resistance arises as a result of electron transfer to the higher conduction-band valleys. We establish a relation between the field at which the negative differential resistance occurs and the precipitate concentration, providing a

0163-1829/95/52(8)/5708(6)/$06.00 ©1995 The American Physical Society

qualitative explanation for the movement of the former to higher fields as the latter is increased. This is related to the presence of an additional scattering mechanism. We demonstrate the comparatively high low-field electron mobility in annealed LT GaAs, a well-established experimental property, although the actual values vary from source to source.[2,8] This spread in available data is found likely to be related to several factors, principally the different precipitate distributions found under different growth conditions and the possibility of parallel conduction paths through the substrate or along the LT GaAs surface.

II. MODEL

The electron transport model implemented here is based on the work of Spicer *et al.*[12] and has been applied to LT GaAs by Warren *et al.*[7] The physical picture of LT GaAs is that As precipitates present in the material are essentially metallic spheres with diameter[13] of about 5 nm (but varying with annealing conditions) embedded in a GaAs matrix. A spherical depletion region forms at the boundary of each sphere and extends into the GaAs as in a planar metal-semiconductor junction.[14] The characteristic widths of the depletion regions are related to the barrier heights, for which values of 0.6–0.7 eV for p-type and 0.7–0.8 eV for n-type GaAs are commonly accepted.[7] The potential outside of the depletion region is given by the following:

$$\Phi(r)=\frac{qN_d}{6\varepsilon_s}\left[\frac{2r_d^3}{r}+r^2-3r_d^2\right], \qquad (1)$$

where N_d is the ionized donor concentration, q is the electron charge, ε_s is the semiconductor permittivity, and r_d is the radius of the depletion region. The depletion-region radius can be calculated from Eq. (1) using the boundary condition of $q\phi(r)=q\phi_b$ at $r=r_0$, where r_0 is the radius of the precipitate and $q\phi_b$ is the barrier height which we take to be 0.7 eV.[15] Note that a range of experimental measurements correspond well with this picture of embedded Schottky barriers, such as photoemission spectroscopy,[9] while other observations such as the very short recombination time are inconclusive.[2]

The key element in our MC calculation of transport properties of LT GaAs is the treatment of electron motion in the regions of inhomogeneous electric field surrounding the precipitate. We have used a semiclassical approach, similar to that adopted by Moglestue in his simulations of small-size semiconductor devices.[16] An individual electron in LT GaAs is accelerated by an external, uniform electric field and by the nonuniform, spatially inhomogeneous internal electric field in the depletion regions while simultaneously experiencing scattering events. Since the electric field surrounding the precipitate is repulsive, the electron is able to move towards the precipitate as long as it has sufficient kinetic energy. The number of precipitates is large and the electron kinetic energy is time varying, so an exact evaluation of electron trajectories for every single depletion region is very computationally intensive and impractically long. We have therefore developed an approach to overcome this problem by using a model in which the electron approaching the precipitate is deflected elastically as from the edge of a hard sphere, of radius r_h that is postulated as the distance from the center of the metal precipitate to the position where the electron potential energy is equal to the mean electron energy.

This hard-sphere approximation has been verified in the limit of low electric field and low precipitate concentration N in the case when the electron distribution function is close to the Boltzmann and the mean kinetic energy of electrons is $\frac{3}{2}kT$. We have calculated the scattering cross section of a single precipitate using the eikonal approximation.[17] The differential transport cross section $\sigma_c(k)$ is then given by

$$\sigma_c(k)=2\pi\int_0^{\pi}|f(\theta)|^2\sin\theta(1-\cos\theta)d\theta , \qquad (2)$$

where θ is the scattering angle, k is the value of the electron wave vector, and $f(\theta)$ is given by

$$f(\theta)=ik\int_0^{\infty}\Im_0(k\theta b)\times\left\{1-\cos\left[\frac{-i}{\hbar v}\int_{-\infty}^{\infty}\phi(b,z)dz\right]\right\}b\,db . \qquad (3)$$

Here $\Im_0$ is the ordinary Bessel function of order 0, $\phi(b,z)=\phi(r)$ is the scattering potential, b is the collision parameter, $v=\hbar k/m^*$, and m^* is the electron effective mass.

The average relaxation time for the scattering by precipitates is given by

$$\langle t\rangle=\frac{\int_0^{\infty}k^{3/2}\exp(-\hbar^2k^2/2m^*)t(k)d^3k}{\int_0^{\infty}k^{3/2}\exp(-\hbar^2k^2/2m^*)d^3k} , \qquad (4)$$

where

$$t(k)=\frac{1}{Nv\sigma_c(i)} . \qquad (5)$$

Such an approach permits a comparison of the mobility due to the scattering by precipitates obtained as a result of the integration of the scattering cross section to the simulated mobility due to the scattering by hard spheres at the same concentration. These two methods should give the same results for low concentration of precipitates, where the event of electron scattering by one precipitate can be considered independent from the scattering by another one. For the experimentally interesting regime of high precipitate concentration, the conventional evaluation of mobility is impossible because of possible correlation of scattering events, while the MC simulation approach remains valid. We found that in order for these two quantities to be identical the radius of the sphere should be $r=8.0r_0$ (r_0 is the precipitate radius) which is close to the radius $r=6.7r_0$ obtained by intersecting the potential energy at the initial value of the mean energy. Such a small discrepancy does not affect the qualitative trends in our results.

The simulation of the individual electron trajectories follows widely used procedures[18,19] in which a sequence

of free flights is generated, each terminated by a scattering event caused by the interaction with phonons or impurities. The scattering processes included in our model are acoustic and optical phonon scattering, inter- and intravalley scattering involving Γ, X, and L conduction-band minima with the nonparabolicity of all three included, and ionized impurity scattering with the compensation ratio also included. The corresponding compensation ratios were deduced from the theoretical model in order to use them for MC calculation. The carrier concentration is $n=N_D^+-N_A^-$, where N_D^+ and N_A^- are the concentrations of ionized donors and acceptors, respectively. The compensation ratio is defined as $\gamma=N_D^+/N_A^-$; accordingly, the total concentration of ionized impurities is related to the compensation ratio by[20]

$$n_{\text{imp}}=n(1+\gamma)/(1-\gamma)\ . \qquad (6)$$

The parameters used for this simulation are taken from Ref. 21.

The scattering by the precipitates modeled by hard spheres was treated from a standpoint different from other scattering mechanisms. During each free flight of duration t_f between scattering events the electron has a certain probability ν of encountering a hard sphere. This probability is related to the size and the concentration of hard spheres which are in turn related to the size, concentration, and spatial distribution of precipitates. Hence each free flight was subjected to interruption by interaction with a hard sphere with a probability ν. For each interrupted flight, a random number r was generated from a uniform distribution to determine the moment of collision $r\times t_f$ with the hard sphere. The act of collision was treated semiclassically. The precipitate size distribution used in the simulation was taken from the histogram given in Ref. 13, curve fitted to provide the distribution. The precipitate spatial distribution is taken to be uniform on the basis of published TEM photographs.[22] We compared the experimental spatial distribution with the uniform distribution using the χ^2 test and a very good agreement was found.

Prior to the simulation the probability ν was determined. Size and spatial distributions and precipitate concentration were used to generate the location of precipitate centers, while the hard-sphere radii were calculated as follows. First Eq. (1) is solved for a given precipitate radius r_0 generated from the size distribution function. Then the radius of the hard sphere, r_h, was determined as the distance at which the potential energy is equal to the electron mean kinetic energy.

As an electron is released and moves due to an electric field, its trajectories may intersect with a hard sphere. The probability of this event, ν, was therefore determined as the ratio of the number of intervals in the trajectories intersected by hard spheres to the total number of intervals in trajectories.

III. RESULTS AND DISCUSSION

First, we discuss the result for compensation ratio zero. We consider the occupancy of Γ, X, and L valleys for various precipitate concentrations, as a function of electric field. The results of our calculations are presented in Fig. 1. As expected, almost all electrons reside in the Γ valley [Fig. 2(a)] at low electric field, while some transfer to higher-lying X and L valleys as the electric field increases [Figs. 1(b) and 1(c)]. The presence of precipitates affects this process significantly, although the overall

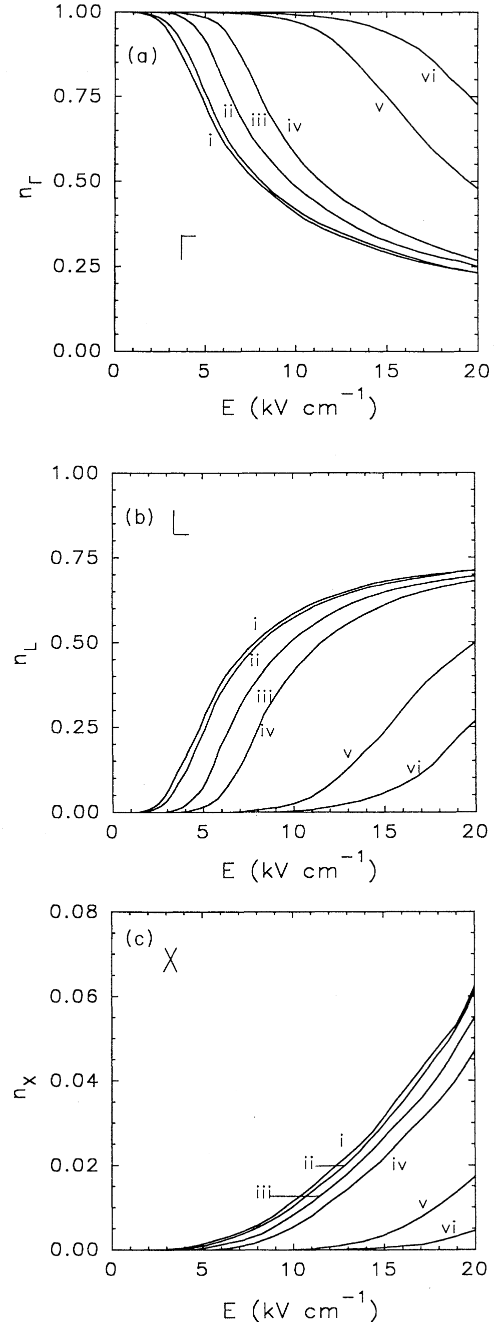

FIG. 1. Fraction of electrons n_Γ, n_X, and n_L in (a) Γ, (b) L, and (c) X valleys as a function of electric field and precipitate concentration. Precipitate concentrations are (i) 0, (ii) 1.0×10^{15} cm^{-3}, (iii) 5.0×10^{15} cm^{-3}, (iv) 1.0×10^{16} cm^{-3}, (v) 5.0×10^{16} cm^{-3}, and (vi) 1.0×10^{17} cm^{-3}.

trend remains. The threshold field at which n_Γ starts to fall increases with increasing precipitate concentration, from an onset field of approximately 2 kV/cm, for GaAs without precipitates, increasing to 9 kV/cm for a precipitate concentration of 1.0×10^{17} cm^{-3}.

Figures 1(b) and 1(c) show the field and precipitate-concentration dependence of the fraction of electrons n_L and n_X in L and X valleys, respectively. In general n_L and n_X continuously increase with increasing field up to 20 kV/cm. For low precipitate concentrations n_L represents a significant fraction of the total electron population of between 50% and 70% above 8 kV/cm, whereas n_X is in the range of 0.5–6% for similar fields. Without precipitates, the electric-field dependence of n_L is slightly different from that calculated by Pozela and Reklaitis.[23] In contrast to their result, our n_L does not decrease for fields above 10 kV/cm, a discrepancy attributable to the different value of intervalley deformation potential preferred in our simulation.

For larger precipitate concentration, n_L increases more slowly. The typical field for which n_L exceeds 5% thus increases quickly with the precipitate concentration, reaching 15 kV/cm for precipitate concentration of 1.0×10^{17} cm^{-3}. Similar behavior can be noticed for the fraction of electrons in the X valley. The onset field at which n_X starts to rise also increases strongly with precipitate concentration, reaching about 14 kV/cm for a precipitate concentration of 1.0×10^{17} cm^{-3}.

In summary, the fraction of electrons in Γ, X, and L valley depends strongly on the precipitate concentration. The addition of precipitate scattering leads to a reduced population in the upper valleys in a similar way to that brought about by additional impurity scattering.[23] For example, the presence of precipitate concentration of 1.0×10^{17} cm^{-3} at 15 kV/cm leads to a decrease in n_L from about 70% to 5%. In the X valley, the decrease is of a similar magnitude but displaced to higher fields and for the same precipitate concentration n_X decreases from 6% to 0.5% at 20 kV/cm, for example. Concurrently, n_Γ decreases as the field increases but the intervalley transfer is moderated by the presence of precipitates, setting in at higher fields for higher precipitate concentrations and markedly reduced in magnitude. For example, at 10 kV/c and with no precipitates, n_Γ is 40% while introducing a precipitate concentration of 1.0×10^{17} cm^{-3} gives a barely noticeable decrease.

Next we discuss the behavior of the drift velocity as a function of electric field for varying precipitate concentration. The principal features, as shown in Fig. 2, are the increase of drift velocity in the Γ valley for electric fields up to 20 kV/cm [Fig. 2(a)] with precipitate-dependent saturation. In satellite valleys [Fig. 2(b)] the drift velocity increases with field and saturation does not occur in the range of fields examined. The overall trend is that the presence of precipitates significantly changes the field dependence of the drift velocity. In the Γ valley [Fig. 2(a)] without precipitates, v_Γ rises rapidly up to fields of 5 kV/cm and then rises more slowly. Other workers[23] predict a small reduction of v_Γ for fields larger than 5 kV/cm again caused by differences in preferred

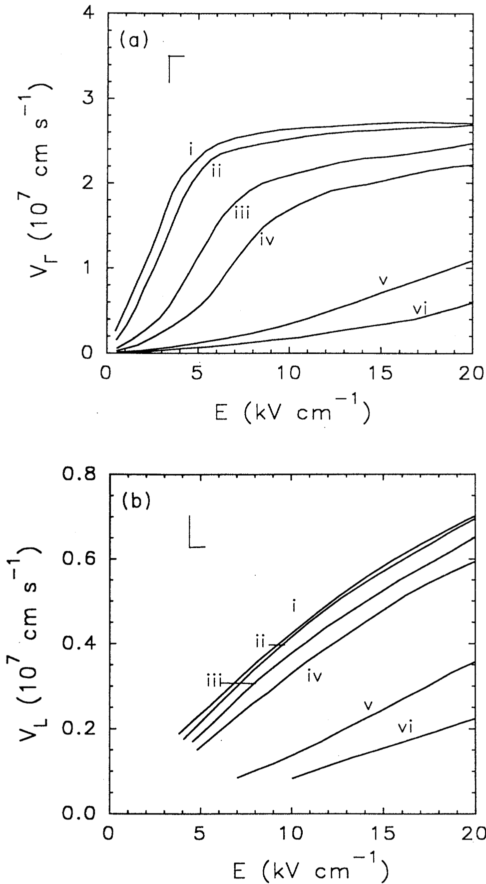

FIG. 2. Drift velocity vs electric field for various precipitate concentrations in (a) Γ valley and (b) L valley. Precipitate concentrations as in Fig. 1.

simulation parameters compared to Ref. 23. The introduction of precipitates reduces v_Γ significantly; a precipitate concentration of 1.0×10^{17} cm^{-3} is sufficient to produce a very small field dependence of v_Γ for fields up to 20 kV/cm.

The drift velocity in L valleys increases monotonically with increasing field [see Fig. 2(b)] and the presence of precipitates again gives a significant reduction. For example, the drift velocity is reduced by a factor of 4 at 15 kV/cm. For low fields, it is difficult to simulate v_L with great accuracy since the average time spent by electrons in the valley is very short.

The average drift velocity was calculated by weighting the drift-velocity components with the fraction of electrons in each valley. Figure 3 shows the calculated drift velocity as a function of field and precipitate concentration for a donor concentration N_d of 1.0×10^{17} cm^{-3} at 300 K, which increases up to a precipitate concentration of about 1.0×10^{16} cm^{-3}. The threshold field for the onset of negative differential mobility is clearly observable. Above about 1.0×10^{16} cm^{-3}, however, it is difficult to observe the onset of negative differential mobility and the drift velocity decreases as the precipitate concentration

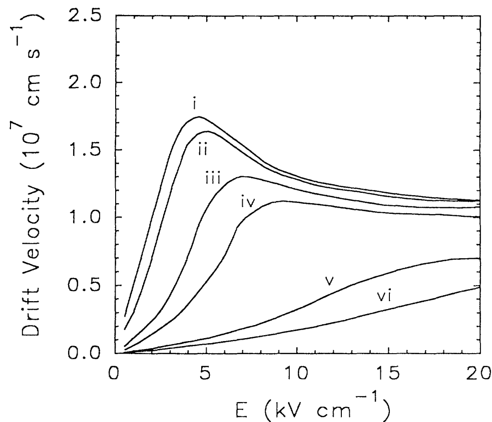

FIG. 3. The average drift velocity as a function of electric field for different precipitate concentrations as in Fig. 1.

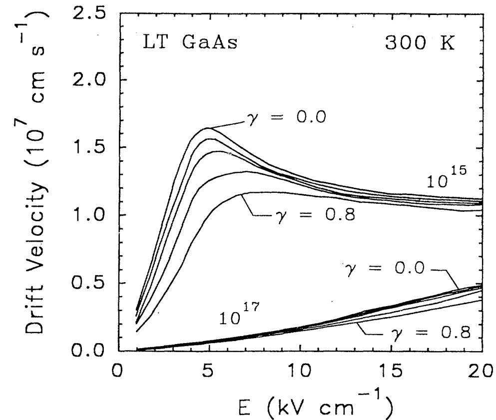

FIG. 5. Drift velocities as a function of electric field for LT GaAs at 300 K for precipitate concentrations of 10^{15} and 10^{17} cm^{-3} and compensation ratio of 0.0, 0.2, 0.4, 0.6, and 0.8, with electron concentration of 10^{17} cm^{-3}.

increases. In the electric-field region where the fraction of electrons in the valleys is close to unity, the drift velocities are almost the same as the drift velocities in the Γ valley. Therefore v_Γ and n_Γ have a key role in governing the drift velocity in the low-field region up to the threshold field.

The field dependence of the drift velocity is related to the electron transfer mechanism. As the electron gains enough kinetic energy, it can be transferred from the central valley to the satellite valleys. In satellite valleys, the electron effective mass is larger than that at the central valley, which leads to a decrease in mobility. In the case of drift-velocity curves in LT GaAs, as the precipitate concentration increases, the probability that an electron is reflected by the precipitate is increased. This effectively reduces the electron mean free path. The reduction is stronger for higher precipitate concentration. Therefore higher electric fields are required at higher precipitate concentration, in order that the electron gains enough energy to reach satellite valleys. This is demonstrated in Fig. 4.

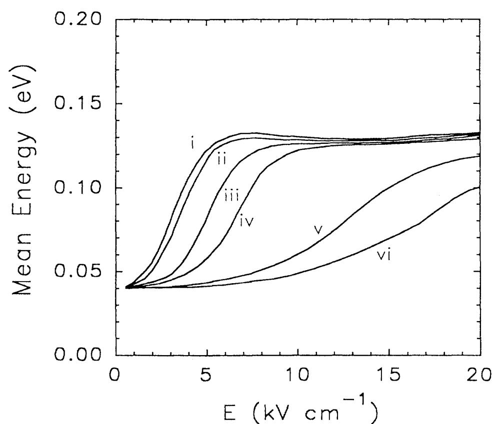

FIG. 4. The electron mean energy vs electric field. Precipitate concentrations as in Fig. 1.

We now turn to the effect of compensation on the drift-velocity characteristics. Figures 5 and 6 show the drift velocity as a function of electric field for various compensation ratios and for precipitate concentration of 10^{15} and 10^{17} cm^{-3} at $T=300$ K and $T=77$ K, respectively. It is clear that at higher precipitate concentration the drift velocity versus field curves are less sensitive to variation of the compensation ratio. The compensation ratio is only dominant for low precipitate concentrations. Compared to the curves at 300 K for precipitate concentration of 10^{15} cm^{-3} (Fig. 5), the curves at 77 K are significantly more sensitive to variation of the compensation ratio. The influence of the compensation ratio on the temperature and precipitate concentration is easy to understand by examining Fig. 7.

Figure 7 shows the value of the drift velocity, taken at a field of 5 kV/cm. It may be noticed that the variation

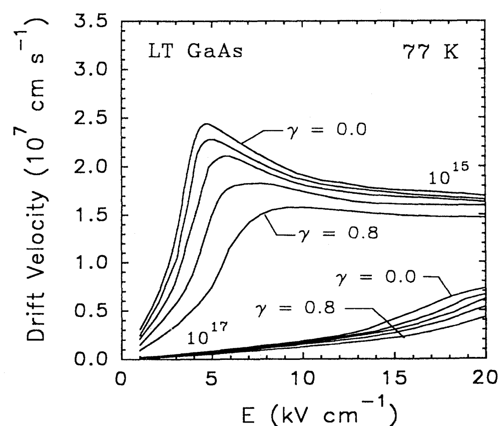

FIG. 6. Drift velocities as a function of electric field for LT GaAs at 77 K for precipitate concentrations of 10^{15} and 10^{17} cm^{-3} and compensation ratio of 0.0, 0.2, 0.4, 0.6, and 0.8, with electron concentration of 10^{17} cm^{-3}.

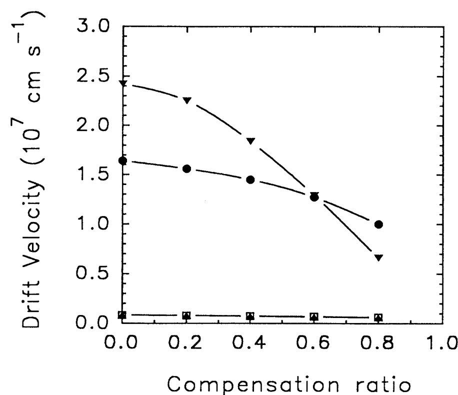

FIG. 7. Compensation-ratio dependence of drift velocity at 5 kV/cm for LT GaAs with precipitate concentration of 10^{15} cm^{-3} at (▼) 77 K and (●) 300 K and precipitate concentration of 10^{17} cm^{-3} at (□) and (▲) 300 K.

of drift velocity (shown by the slope of each curve) is larger at low precipitate concentration. At higher precipitate concentration, this variation is fairly small. For low precipitate concentration, as the temperature decreases to 77 K, the dependence of *V-F* curves on compensation ratio becomes stronger.

IV. SUMMARY

We have studied the electron transport in LT GaAs using the Monte Carlo approach in the framework of the buried Schottky diode model. We used an approach of introducing a hard-sphere approximation to overcome the problem of non-uniform electric field surrounding the precipitates. The advantage of this approach is that the effect of scattering by a large concentration of precipitates can be included as opposed to the standard method based on the scattering cross sections. The results obtained by our simulation for low precipitate concentration coincide with the calculations based on the precipitate scattering cross section in the eikonal approximation. In our simulation the electron trajectory in real space was generated and the validity of this approach was tested by calculating the drift velocity of homogeneous GaAs where excellent agreement was reached. We have evaluated the drift velocity and the electron occupancy in Γ, X, and L valleys in LT GaAs as a function of precipitate concentration and electric field. The calculations show that the presence of precipitates in LT GaAs has a dramatic impact on the drift velocity and on the electron population in higher valleys at high electric fields. The principal reason is that particularly at low energies the precipitates act as scattering centers and a certain fraction of the crystal volume is occupied by depletion regions to which electrons have limited access. This changes the electron mean free path considerably and prevents electrons from being transferred to higher valleys, which is eventually achieved at much higher fields than for homogeneous GaAs. Increased compensation ratio generally reduces the drift velocity; however, it only has a significant effect at low precipitate concentrations and at low temperatures.

[1]A. C. Warren, J. M. Woodall, J. H. Burroughes, P. D. Kirchner, H. K. Heinrich, G. Arjavalingam, N. Katzenellenbogen, D. Grischkowsky, M. R. Melloch, N. Otsuka, K. Mahalingam, F. H. Pollak, and X. Yin, in *Low Temperature (LT) GaAs and Related Materials,* edited by G. L. Witt, R. Calawa, U. Mishra, and E. Weber, MRS Symposia Proceedings No. 241 (Materials Research Society, Pittsburgh, 1992), p. 15.
[2]S. Gupta, M. Y. Frankel, J. A. Valdmanis, J. F. Whittaker, G. A. Mouron, F. W. Smith, and A. R. Calawa, Appl. Phys. Lett. **59**, 3276 (1991).
[3]Kim Man Yu, M. Kaminska, and Z. Liliental-Weber, J. Appl. Phys. **72**, 2850 (1992).
[4]Z.Q. Fang and D. C. Look, Appl. Phys. Lett. **63**, 219 (1993).
[5]M. O. Manasreh, D. C. Look, K. R. Evans, and C. E. Stutz, in *Proceedings of the 6th Conference on Semi-Insulating III-V Materials, Toronto, 1990,* edited by A. G. Milnes and C. J. Miner (Hilger, Bristol, 1990), p. 105.
[6]Z. Liliental-Weber, A. Claverie, J. Washburn, F. W. Smith, and A. R. Calawa, Appl. Phys. A **53**, 141 (1991).
[7]A. C. Warren, J. M. Woodall, J. L. Freeouf, D. Grischkovsky, D. T. McInturff, M. R. Melloch, and N. Otsuka, Appl. Phys. Lett. **57**, 1331 (1990).
[8]A. C. Warren, J. M. Woodall, P. D. Kirchner, X. Yu, F. Pollak, M. R. Melloch, N. Otsuka, and K. Mahalingam, Phys. Rev. B **46**, 4617 (1992).
[9]D. T. Inturff, J. M. Woodall, A. C. Warren, N. Braslau, G. D. Petit, P. D. Kirchner, and M. R. Melloch, Appl. Phys. Lett. **60**, 448 (1992).
[10]Y. Chen, S. Williamson, T. Brock, F. W. Smith, and A.R. Calawa, Appl. Phys. Lett. **59**, 1984 (1991).
[11]T. Motet, J. Nees, S. Williamson, and G. Morou, Appl. Phys. Lett. **59**, 1455 (1991).
[12]W. E. Spicer, P. W. Chye, P. R. Skeath, C. Y. Su, and I. Lindau, J. Vac. Sci. Technol. **16**, 1422 (1979).
[13]K. Mahalingam, N. Otsuka, M. R. Melloch, J. M. Woodall, and A. C. Warren, J. Vac. Sci. Technol. B **9**, 2328 (1991).
[14]S. M. Sze, *Physics of Semiconductor Devices* (Wiley, New York, 1981).
[15]D. V. Rossi, E. R. Fossum, G. D. Pettit, P. D. Kirchner, and J. M. Woodall, J. Vac. Sci. Technol. B **5**, 982 (1987).
[16]C. Moglestue, Rep. Prog. Phys. **53**, 1333 (1990).
[17]L. I. Schiff, *Quantum Mechanics,* 3rd ed. (McGraw-Hill, New York, 1968), p. 338.
[18]W. Fawcett, A. D. Boardman, and S. Swain, J. Phys. Chem. Solids **31**, 1963 (1970).
[19]J. C. Jacoboni and L. Reggiani, Rev. Mod. Phys. **55**, 645 (1983).
[20]J. W. Walukiewicz, L. Lagowski, L. Jastrzebski, M. Lichtensteiger, and H. C. Gatos, J. Appl. Phys. **50**, 899 (1979).
[21]K. Hess, *Advanced Theory of Semiconductor Devices* (Prentice-Hall, Englewood Cliffs, NJ, 1988).
[22]M. Melloch, J. Woodall, N. Otsuka, and D. Nolte, III-V Rev. **6**, 46 (1993).
[23]J. Pozela and A. Reklaitis, Solid State Electron. **23**, 927 (1980).